THE JOURNAL OF PHYSICAL CHEMISTRY B

Article

pubs.acs.org/JPCB

The Effects of Template Rigidity and Amino Acid Type on Heterogeneous Calcium-Phosphate Mineralization by Langmuir Films of Amphiphilic and Acidic β-Sheet Peptides

Shlomit Segman-Magidovich and Hanna Rapaport*

The Avram and Stella Goldstein-Goren Department of Biotechnology Engineering and the Ilse Katz Institute for Nanoscale Science and Technology, Ben-Gurion University of the Negev, Beer-Sheva 84105, Israel

ABSTRACT: Calcium-phosphate mineralization was monitored in systems composed of designed amphiphilic and acidic β-sheet-forming peptides, namely Pro-Phe-$(Asp\text{-}Phe)_5$-Pro (PFD-5), Pro-Phe-$(Glu\text{-}Phe)_5$-Pro (PFE-5) and Pro-Glu-$(Phe\text{-}PSer)_4$-Phe-Glu-Pro (PPS). The three peptides differ solely in terms of their hydrophilic amino acids and therefore, serve as good model for assessment of the effect of the anionic amino acid type on mineralization within the context of the β-sheet structure. Monolayers of the peptides were deposited over simulated body solution ($SBF_{1.5}$), and the effect of the adsorbing minerals over time was detected by Langmuir isotherm measurements, grazing incidence X-ray diffraction (GIXD) and Brewster angle microscopy (BAM). The results provide insight into mineralized film morphology and peptide lattice behavior during mineralization. The rigidity of the peptide template, along with the type of amino acid side chain, were found to significantly affect mineralization morphology and peptide structure. The results will contribute to a better understanding of calcium-phosphate mineralization in nature and in the context of biomaterials for applications in bone tissue regeneration.

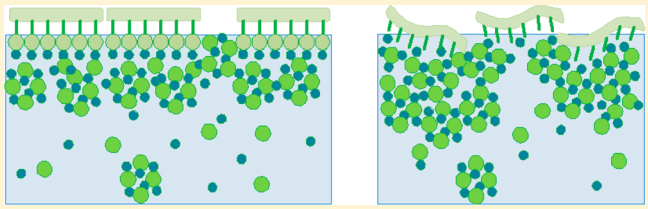

INTRODUCTION

The formation of biominerals in nature is controlled by organic molecules, proteins, and polysaccharides in such manners that lead to the appearance of unique shapes with distinct chemical and physical properties. It is believed that biomolecules induce the nucleation of inorganic materials and assist in shaping the growth and development of biominerals. Understanding the principles underlying those processes involved in biomineralization thus holds great promise for the design and synthesis of bioinspired mineralized materials.

Proteins rich in acidic amino acids have been proposed to participate in the nucleation and growth of carbonated apatite.[1,2] Electrostatic interactions induced by negatively charged residues of such proteins clearly play an important role in controlling ionic adsorption and thus the form of template-induced crystal growth.[3,4] In recent years, it has been established that the concept of epitaxy, or mineralization induced by a structural match between the interfaces of a template presenting arrayed functional groups and that of the nucleating crystal, is limited to specific systems and conditions.[5] In this context, the involvement of amorphous mineral phases in the early stages of biomineralization[6−8] has been demonstrated in systems of amorphous calcium carbonate, as well as amorphous calcium phosphate forms, in mineralized species,[9,10] enamel,[7] bones,[11] and in biomimetic systems.[12]

Various studies have employed peptide systems with certain secondary structures to induce and monitor mineralization in the presence of defined molecular templates.[13−18] Peptides belonging to a family of amphiphilic and acidic β-sheet molecules may assemble as monolayers at the air−water interface, with hydrophobic side chains pointing into the air and hydrophilic side chains oriented on the opposite side, into the aqueous subphase. Such monolayers found at interfaces may serve as a model in mineralization studies, whereby the molecular layer induces adsorption of ions from the solution and the further growth of the mineral phase. Recently, the flexibility of a monolayer template in a β-sheet structure present at the interface of a saturated calcium carbonate solution was shown to induce a unique shape of calcite crystals.[19] In addition, a monomolecular film composed of the peptide, Pro-Asp-$(Phe\text{-}Asp)_5$-Pro, denoted PFD-5, was used to induce calcium-phosphate mineralization.[20] This study revealed that the PFD-5 monolayer found at the interface of simulated body solution ($SBF_{1.5}$) first adsorbed calcium-phosphate in the amorphous state that had transferred into the developed hydroxyapatite form over time.

Here, we aimed to monitor in situ calcium-phosphate mineralization induced by amphiphilic and acidic β-sheet peptides with grazing incidence X-ray diffraction (GIXD), an approach that provides structural information of crystalline films at the air−water solution interface.[21] GIXD patterns from various amphiphilic β-sheet peptides forming monolayers at interfaces[22] were, in general, found to display two main Bragg peaks: one that is associated with peptide length, and the other presenting interstrand spacing that is determined by hydrogen bonds linking neighboring strands within the β-sheet assembly

Received: June 1, 2012
Revised: August 8, 2012
Published: August 9, 2012

(Scheme 1). Moreover, GIXD measurements of the peptide monolayers belonging to this family of peptides, as for example

Scheme 1. Compression on Langmuir films of the β-Sheet Peptides Leading to a Shift in Bragg Peak Position[23,24] as Detected by GIXD Measurements[a]

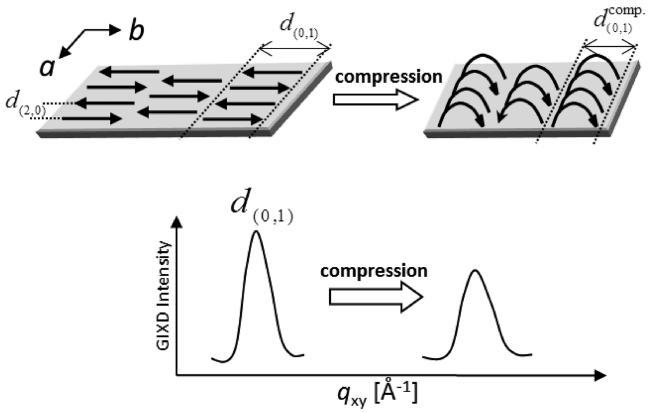

[a]Top: The two-dimensional peptide assembly shown schematically with arrows representing the β-strands. The spacings indicate the two main Bragg peaks usually detected: one that corresponds to the peptide length assigned as $d_{(0,1)}$, and the other the inter-strand hydrogen bond distance, assigned as $d_{(2,0)}$. Bottom: Schematic representation of the shift in $d_{(0,1)}$ peak position upon Langmuir monolayer compression.

Pro-Glu-(Phe-Glu)$_5$-Pro (PFE-5), indicated that the repeat distance generated by the peptides long axes, $d_{(0,1)}$, may decrease in length by more than 30%,[23] as a result of high crystalline monolayer compressibility.

In this study, we monitored calcium-phosphate mineralization induced by the PFD-5, PFE-5, and Pro-Glu-(Phe-PSer)$_4$-Phe-Glu-Pro (PPS) peptide (see Scheme 2) monolayers spread over simulated body solution (SBF$_{1.5}$) using Langmuir isotherms, Brewster angle microscopy (BAM), and GIXD to evaluate the effect of mineralization on structural characteristics of the peptide film. Mineralized films were also transferred to solid support and scanned by IR spectroscopy. These three peptides differ only in their hydrophilic amino acids and, therefore, serve as good models for assesmment of the effect of anionic amino acid type on mineralization within the context of the β-sheet structure.

EXPERIMENTAL SECTION

Materials. Peptides were custom synthesized and purified by high-performance liquid chromatography (HPLC) to 95% by AnaSpec (Fremont, CA) and Novetide (Haifa, Israel).

Methods. Surface pressure−area (π−A) isotherms. The isotherms of peptide monolayers were measured using a KSV minitrough (KSV Instruments, Helsinki, Finland) on deionized water and on the mineralizing solution, i.e., simulated body fluid (SBF$_{1.5}$, see below) at 25 °C. Monolayers of peptides were prepared by spreading a ∼0.1 mg/mL solution of each peptide, dissolved in trifluoroacetic acid/chloroform (1:9 (v/v)). All monolayers films were deposited to a mean area per molecule of ∼220 Å^2. The mean molecular area (A) is the area available on the Langmuir trough divided by the number of molecules spread. Note that the area per molecule in the π−A isotherms may be influenced by various factors, including aggregation of the peptide in the stock solution used for spreading the film at

Scheme 2. Sequences of the Three Peptides Studied That Differ Only in the Nature of Their Hydrophilic Residues[a]

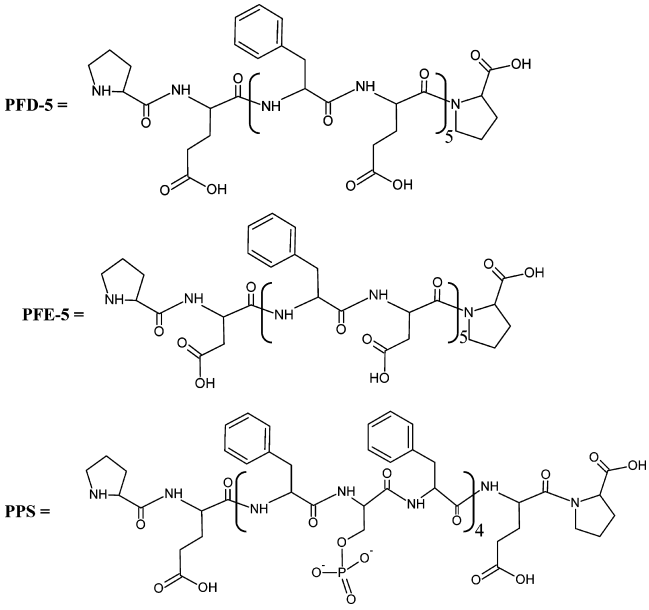

[a]The peptides were designed according to the general formula, Pro-Y-(Z-Y)$_5$-Pro, with Y being negatively charged and Z being hydrophobic amino acids.

the interface, peptide content in the lyophilized peptide stock powder used in the spreading solution, peptide purity, and its possible dissolution in the subphase. Consequently, Langmuir isotherms of the peptides may show areas per molecule that are smaller than those expected, based on the assumed molecular projected area. TFA used in the spreading solution in isotherms of peptides measured on deionized water may lead to a drop in pH of the subphase to ∼3.5−4. The lower pH is not expected to lead to change in the ionization state of the hydrophilic amino acids that are assumed to be protonated[22] and thus has no effect on area per molecule. In control experiments, Langmuir isotherms of peptides following 18 h of incubation on deionized water show negligible differences with slightly smaller limiting area per molecule, compared to those obtained prior to the incubation.

Simulated Body Fluid (SBF$_{1.5}$). This buffered mineralization solution constitutes the various ions of human blood plasma at 1.5 times their physiological concentration, so as to expedite the mineralization process. The solution and its preparation are based on Kokubo's method.[25] Briefly, NaCl (213 mM), $NaHCO_3$ (6.3 mM), KCl (3.5 mM), K_2HPO_4 (1.5 mM), $MgCl_2$ (2.3 mM), $CaCl_2{\cdot}2H_2O$ (3.8 mM) and Na_2SO_4 (0.75 mM) were dissolved consecutively in double-distilled water at 36 °C and buffered at pH 7.35 using 75 mM tris-(hydroxymethyl)aminomethane, along with an appropriate volume of 1 M HCl. The solution was stored for 24 h at 4 °C in polypropylene flasks prior to the experiments, to allow for equilibrium to be reached. This solution, which shows negligeble mineralization at its interface with humidified air, over a period of 20 days,[20] was used as a subphase in the mineralization studies of the peptide monolayers.

Grazing Incidence X-ray Diffraction. GIXD experiments were performed using the liquid surface diffractometer at the BW1 undulator beamline at the HASYLAB synchrotron source (Hamburg, Germany). Peptide films were spread at room

dx.doi.org/10.1021/jp305386e | J. Phys. Chem. B 2012, 116, 11197−11204

temperature, and diffraction measurements were performed at 25 °C. A monochromatic X-ray beam (λ = 1.3039 Å) was adjusted to strike the liquid surface at an incident grazing angle of $\alpha_i \approx 0.85\alpha_c$, where α_c is the critical angle for total external reflection. This angle was selected as it enhances surface sensitivity. GIXD signals were obtained from two-dimensional crystallites randomly oriented about the water surface normal. The scattered intensity was collected by means of a position-sensitive detector, which intercepts photons over the range 0.0 $\leq q_z \leq$ 1.3 Å^{-1}, with $q_z \cong 2\pi/\lambda \sin(\alpha_f)$ being the out-of-plane component of the scattering vector and α_f being the exit vertical angle. Measurements were performed by scanning $2\theta_{xy}$, namely, the angle between the projections onto the horizontal plane of the incident and diffracted beams, with $q_{xy} \cong 4\pi/\lambda \sin(2\theta_{xy})$ being the in-plane scattering vector. The q_{xy} positions of the Bragg peaks yield the lattice spacings $d = 2\pi/q_{xy}$, which may be indexed by the two Miller indices, h and k, to yield a unit cell. In the present study, focus was placed on Bragg peaks corresponding to the peptide length, which have previously been indexed, $d_{(0,1)}$.[23,24] GIXD measurements were performed with peptide monolayers on water and on $SBF_{1.5}$. Due to limitations on synchrotron time availability, the incubation time for the mineralization study was chosen as 5 h as apposed to 18 h in Langmuir isotherms measurements. During the 5 h incubation, a measurable increase in surface pressure was already detected for PFE-5 and PPS on $SBF_{1.5}$.

In Langmuir isotherms of monolayers in general, the change in mean molecular area, A, as a function of surface pressure, π, namely $C_M = -\partial(\ln A)/\partial\pi$, measures the compressibility of the film. We have shown that for PFD-5 and PFE-5 and in general for similar β-sheet amphiphilic peptides of this family, the change in d(0,1) may offer a measure of the area of the peptides within the lattice so that the crystalline compressibility of the two-dimensional lattice, C_C, may be estimated by $C_C = -\partial(\ln d_{(0.1)})/\partial\pi$. Thus, the π–A compression Langmuir isotherms that are presented as π versus ln A can be fitted with linear equations. The inverse of the linear line slope is equal to the macroscopic compressibility of the monolayer, C_M. For example, a slope of −87.9 mN/m corresponds to C_M = 1/(87.9 mN/m) × 1000(mN/1N) = 11.4 m/N.[24] Compressibility of the crystalline monolayer peptide structure, which manifests in shrinkage of the $d_{(0,1)}$ spacing, may be evaluated as $C_C = -(\partial \ln d_{(0,1)}/\partial\pi)$, the slope of π versus ln $d_{(0,1)}$.

FTIR spectra were measured on a Bruker EQUINOX 55 instrument equipped with a mercury–cadmium–telluride detector at 2 cm^{-1} resolution under a nitrogen atmosphere. Monolayers of the peptides were prepared at the air–water interface and transferred to a 45° ATR ZnSe prism face, which was manually lowered in a horizontal orientation until the prism face touched the water surface. The same transfer procedure was repeated for the opposite face of the ZnSe prism. The ATR crystal was mounted on a vertically oriented ATR bench. A total of 1000 scans were averaged for each spectrum. Peptide films were incubated over the SBF solution[20] for 12 days in a humidified incubator at 37 °C to expedite the mineralization and allow its detection by the FTIR measurements.

Brewster Angle Microscope. A Brewster angle microscope (NFT, Gottingen, Germany) mounted on a Langmuir film balance was used to observe the microscopic structures in situ at the air/water interface at 25 °C . The light source of the BAM was a frequency-doubled Nd:YAG laser with a wavelength of 532 nm and 20–70 mW primary output power in a collimated beam. BAM images were recorded with a charge-coupled device (CCD) camera. The scanner objective was a Nikon superlong working distance objective with a nominal 10× magnification and a diffraction-limited lateral resolution of 2 μm. The images were corrected to eliminate side ratio distortion originating from the nonperpendicular line of vision of the microscope.

RESULTS

Langmuir Isotherms. The three amphiphilic and acidic peptides form stable monolayers at the interface of water with isotherms that generally exhibit the pattern typical of this family of peptides. The isotherms start at a low surface pressure in the expanded state, followed by a steep increase in surface pressure along a region that is denoted as the compressed state, that ends with collapse and surface pressure leveling off. Differences in isotherm patterns on water and on $SBF_{1.5}$ are indicative of interactions of the peptide monolayers with the $SBF_{1.5}$ solution. These differences are revealed in limiting area per molecule (Figure 1), and compressibility of the monolayer at the compressed and collapsed states. The three peptides, comprising 13 amino acids each, should theoretically have

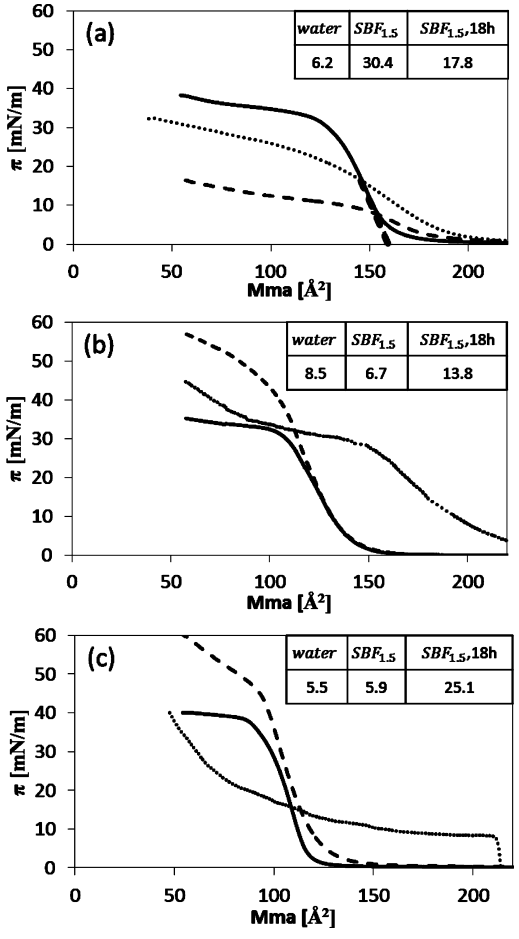

Figure 1. Surface pressure–area isotherms of (a) PFD-5, (b) PFE-5, and (c) PPS on water (solid line), on $SBF_{1.5}$ (dashed line), and on $SBF_{1.5}$ following 18 h of incubation prior to compression (dotted line). A dashed line drawn tangent to the steepest slope along the compressed state is used to determine the limiting area per molecule, the point at which the peptides are essentially closely packed and fully covering the interface.

dx.doi.org/10.1021/jp305386e | J. Phys. Chem. B 2012, 116, 11197–11204

shown the same limiting molecular area on deionized water, i.e., 13 × ~16.4 = 213 Å ^{2} (where 16.4 Å^2 is the projected area an amino acid occupies in a β-sheet structure[22] with an assumed 6.9 Å distance between every second amino acid along the strand and a 4.75 Å distance between strands; see Scheme 1). Nonetheless, differences in the amounts of residual water or soluble salts in the purified peptide (see Experimental Section) may lead to shifts in the limiting area per molecule, as extracted from the isotherm. Hence, for each peptide, the isotherms measured on water subphase served as a reference for those obtained for the same peptide on $SBF_{1.5}$ and on that solution following overnight incubation. The limiting area per molecule of PFD-5, PFE-5 and PPS are A = 160, 140, and 120 Å^2, respectively (Figure 1). The isotherms of PFD-5 and PPS on $SBF_{1.5}$-NI (where NI assigns - with no incubation) display a small shift to higher limiting molecular areas, compared to the corresponding isotherms obtained on water, pointing to interactions with the ions in the $SBF_{1.5}$ subphase. The corresponding isotherm of PFE-5 shows a limiting area per molecule that coincides with that obtained on water but with differences in the collapse state. The compressibility of peptides, PFE-5 and PPS monolayers along the compressed state, C_M, (Figure 1a–c, insets), indicate quite similar values on water (8.5 and 5.5 m/N) and on $SBF_{1.5}$-NI (6.7 and 5.9 m/N), respectively. PFD-5, however, shows a quite large increase in monolayer compressibility on $SBF_{1.5}$, as compared to that on water (30.4 versus 6.2 m/N, respectively). Nevertheless, PFD-5 appeared to have formed an unstable film on $SBF_{1.5}$-NI, reflected in the large decrease in collapse surface pressure. Accordingly, in this case, the value determined by the slope of the isotherm may be affected by the relatively early collapse. The compressibility of all peptides measured on $SBF_{1.5}$-NI along the collapsed state is smaller than that on water, as manifested by the elevated slope of the isotherms along this region in comparison to the slope of the isotherms along the collapsed state on water. These differences point to interactions of all the three peptides with the $SBF_{1.5}$ solution that occur already along the relatively short period of time of these experiments. Following incubation of the peptide films on $SBF_{1.5}$ for 18 h, all isotherms appeared significantly different, as compared to those obtained on the solution with no incubation. The peptides showed an increase in surface pressure in the most expanded state where these were left for incubation. The most prominent increase in the initial surface pressure was evident for the PPS peptide, followed by PFE-5, with $\pi \sim 8$ and ~4 mN/m, respectively (Figure 1b,c). Interestingly, the isotherm of the incubated PPS shows large compressibility as in the expanded state down to an area per molecule at ~100 Å^2 (determined by tangent line to the steepest slope along the following compressed state) that is quite similar to the limiting area per molecule obtained on water and on $SBF_{1.5}$-NI. By contrast, the PFE-5 shows a compressed state that starts already in the most expanded state of the film, where it was left for incubation. These differences between incubated PFE-5 and PPS may point to differences in the mineralized films characteristics formed by the two peptides. The compressibility of all three peptides incubated on $SBF_{1.5}$, along the compressed states, measured as 17.8, 13.8, and 25.1 m/N for PFD-5, PFE-5, and PPS, respectively, was higher than that on water and on $SBF_{1.5}$-NI, except for that obtained with PFD-5, which already formed an unstable, highly compressible film on $SBF_{1.5}$-NI.

Brewster Angle Microscopy. A series of BAM images was acquired along the compression isotherms (Figure 2). The

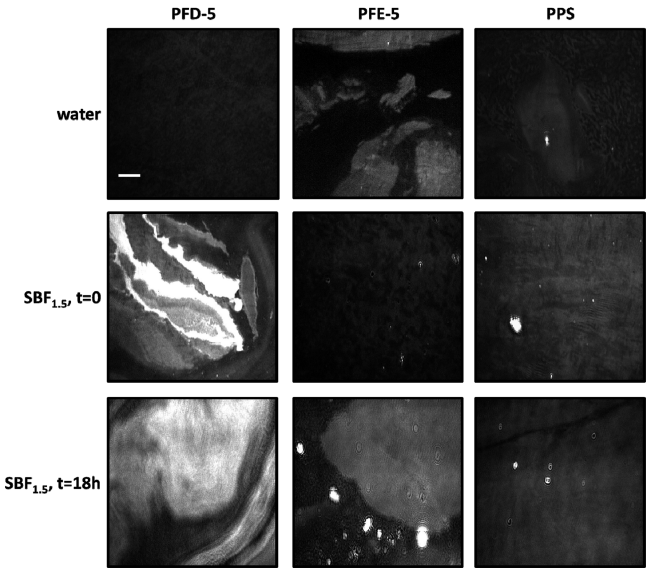

Figure 2. BAM images of Langmuir peptide monolayer films on water, $SBF_{1.5}$-NI, and on $SBF_{1.5}$ after 18 h of incubation. Images were acquired in the expanded state of the trough, in accordance with the initial area/molecule stated above in the isotherms (scale bar = 50 μm).

images visualized the mineralization process taking place at the peptide films a short time after film deposition on $SBF_{1.5}$-NI and on the same solution after 18 h of incubation. It is well established that the gray levels in BAM images correlate with film thickness and/or molecular orientation, with brighter gray values indicative of thicker film. In the case of the peptides studied here, changes in molecular orientation are not highly probable, as the peptides are held by an equivalent number of hydrogen bonds on both sides of the strands. Thus, it is more likely that those regions appearing brighter in BAM reflect thickening of the film due to either film collapse and/or accumulation of the mineralizing ions. Indeed, films of peptides spread on deionized water at the collapse state show a higher intensity of reflected light that is indicative of the thicker film generated following the compression (not shown). Comparing the images obtained on water with those obtained on $SBF_{1.5}$-NI, PFD-5 appears to undergo the most dramatic change in film texture, pointing to excessive ionic adsorption occurring already a short time after peptide deposition at the interface. The images of PFE-5 and PPS on $SBF_{1.5}$-NI appear to be more similar to those obtained on water, suggesting interactions with the ions in the subphase are either slower or less excessive, and in any event, less disruptive to film texture. Comparing the images of films incubated for 18 h on $SBF_{1.5}$ to those of $SBF_{1.5}$-NI, it appears that the PFD-5 monolayer induced thicker mineral deposition and apparently it led to more deformable-mineralized film than did PFE-5 or PPS. The PPS film after 18 h appears flat and rigid and quite similar to the $SBF_{1.5}$-NI film.

Grazing Incidence X-ray Diffraction. GIXD measurements of the peptide monolayers, performed along the compression isotherm, generally yield two distinct Bragg peaks (Scheme 1), with one arising from order along the β–strand long axis. This spacing, which usually corresponds to the projected length of the peptide along the backbone in these

dx.doi.org/10.1021/jp305386e | J. Phys. Chem. B 2012, 116, 11197–11204

peptide systems, is assigned as $d_{(0,1)}$. On the basis of the commonly detected dimensions of pleated β-strands in which every other amino acid is 6.9 Å away, the estimated length of the peptide is 13 × 6.9/2 ∼ 45 Å. In some peptide we previously characterized, this spacing has been found to correspond to a length that is longer than a single peptide,[24] implying that the peptides in such a case generated a lattice in which at least two peptides give rise to this repeat distance. Here, we aimed to gain insight into the effect of calcium-phosphate mineralization on the peptide lattice, as reflected in the position of the $d_{(0,1)}$ peak, which previously was shown to be highly sensitive to compression state, shifting to lower spacings in reponse to an increase in surface pressure (Scheme 1). That shift is used for calculating the crystalline compressibility, C_C (see Experimental). GIXD measurements were performed along film compression for peptides on water and on $SBF_{1.5}$ immediately after film deposition (similar to conditions used above with $SBF_{1.5}$-NI), and after 5 h of incubation on this ionic solution.

GIXD measurements were carried with the purpose of obtaining the crystalline compressibility of the peptide monolayers, along the compressed state on water as a reference for the same measurements on the $SBF_{1.5}$ solution. The crystalline compressibility of PFD-5 along the compressed state on water (Figure 3 and Table 1) was found to be C_C = 7.4 m/N, close to the 8.7 m/N value we previously reported[24] for this peptide and almost identical to that found for PFE-5.[23] These small differences in crystalline compressibility, in the range of ∼ ± 1 m/N, between values found here compared to those reported before for PFD-5, are reasonable in view of peptide purity (95%) and other minor aspects of the experimental conditions used.[24] In contrast to the rather similar crystalline compressibility values of these two peptides, the PPS monolayer on water was found to form a much more rigid crystalline assembly. This peptide apparently crystallized along the compressed state, on compression of the film to a π value of ∼4.2 mN/m. The detected $d_{(0,1)}$ spacing of PPS on water, corresponding to 42 Å (Table 1 and Figure 3), shifted only to 41 Å with increase in surface pressure to π ∼ 8.6 mN/m. Upon further compression to 19 mN/m, there was essentially no change in this spacing. These results indicate that the PPS strands cannot be compressed any further then the 41 Å under the conditions generated along the Langmuir isotherm. Thus, peptide PPS forms a unique assembly, which behaves as a uncompressible crystalline two-dimensional solid.

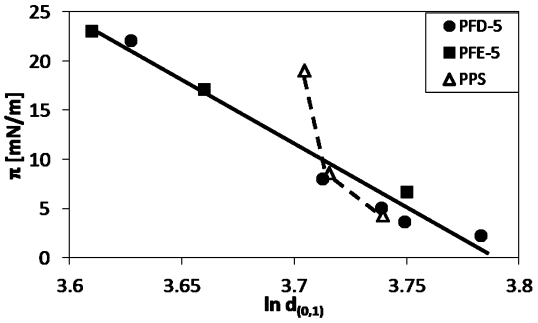

Figure 3. ln $d_{(0,1)}$ versus surface pressure for peptide monolayers on water measured along compression. The slope of the line that goes through the PFD-5 and PFE-5 values represents the average compressibility, 7.6 m/N, of these two peptides (see text). The compression of PPS was not extended further since there was no significant change in peak position over the rather large change in surface pressure (see data in Table 1).

Table 1. Summary of GIXD Data Obtained for Peptide Monolayers along Film Compression on Water and on $SBF_{1.5}$[a]

PFD-5			PFE-5			PPS		
π [mN/m]	$d_{(0,1)}$ [Å]	ln $d_{(0,1)}$	π [mN/m]	$d_{(0,1)}$ [Å]	ln $d_{(0,1)}$	π [mN/m]	$d_{(0,1)}$ [Å]	ln $d_{(0,1)}$
2.2	43.9	3.78	1.4	46	3.82	4.2	42.0	3.74
3.6	42.4	3.74	6.7	42.6	3.75	8.6	41.0	3.71
5.0	42.0	3.73	17.1	38.9	3.66	19	40.6	3.70
8.0	40.9	3.71	23.0	37.1	3.61			
22.1	37.6	3.62						
				on $SBF_{1.5}$				
0.9	57.7	4.05	0	55.6	4.02	0.7	52.3	3.96
1.7	56.6	4.03	0	55.0	4.01	1.1	52.0	3.95
			0.6	53.6	3.98	2.2	50.7	3.93
			[b]0.8	54.0	3.99	[b]7.0	50.4	3.92

[a]The results of PFE-5 on water were previously reported. [23] The table presents the $d_{(0,1)}$ spacing corresponding to the detected Bragg peaks and the corresponding ln $d_{(0,1)}$ values used in evaluating crystalline compressibility (see Experimental Section and Figure 3). [b]Assigns data obtained after 5 h of monolayer incubation on $SBF_{1.5}$, in the state detailed in the preceding raw, demonstrating the increase in surface pressure due to continual mineralization of the film and the correspondingly measured $d_{(0,1)}$ spacing, which in case of PFD-5, could no longer be detected.

GIXD of the peptide films deposited on the $SBF_{1.5}$ was measured along a small region of compression immediately after film deposition so as to detect the presence of the ordered film and confirm its expected crystalline compressibility at the solution interface. Specifically, it was deemed of interest to detect the effect of the growing mineralized layer on the peptide films (see Experimental Section), following a few hours of incubation on the mineralizing solution and to compare the compressibility of the mineralized peptide to that obtained on water. Hence, the film was left for a 5 h incubation over the $SBF_{1.5}$ solution, at which point GIXD was again measured. Noteworthy, in all GIXD measurements performed with the peptides on the mineralizing solution the diffraction peaks were only from the peptide films in accordance with the amorphous nature typical to the early stages of calcium phosphate adsorption and mineralization.[20] PFD-5 monolayer deposited on the $SBF_{1.5}$ solution showed $d_{(0,1)}$ spacing of 57.7 Å, a value quite similar to spacing previously detected (60.5 Å) for this peptide on water, which was, however, obtained following compression and expansion cycle of the Langmuir film.[24] This spacing, which is longer than the length of a single peptide, suggests that in the present system, the interactions of PFD-5 with the $SBF_{1.5}$ ions altered the packing arrangement of the peptides, as compared to the packing obtained on water, yielding a lattice that is likely containing two molecules per repeat distance, along the strand direction. Following a small compression and the accompanying increase in surface pressure (Table 1), the lattice was slightly modified to yield a spacing of 56.6 Å and at this stage, the film was left for a 5 h incubation. Following the incubation, no GIXD peaks could be detected for this peptide, implying that the continuing interactions of the monolayer with the mineralizing solution disrupted the peptide order that was observed prior to incubation. Peptide PFE-5 on $SBF_{1.5}$ showed 55.6 Å spacing, similar to that of PFD-5 on the

dx.doi.org/10.1021/jp305386e | J. Phys. Chem. B 2012, 116, 11197−11204

same solution, and that upon slight compression shifted to 53.6 Å (Table 1), in accordance with the expected crystalline compressibility of the lattice at this state. Following the period of incubation, there was a small increase in surface pressure, indicative of mineralization and ions becoming adsorbed to the peptide. The $d_{(0,1)}$ spacing, however, remained essentially the same at 54.0 Å, suggesting that the peptide template is more resistant than that of PFD-5 to interactions with the mineralizing solution, maintaining the integrity of the diffracting domains along the mineralization. PPS on $SBF_{1.5}$ generated a lattice with ∼52 Å spacing, a value that upon slight compression decreased to 50.7 Å. It is likely that this peptide, as did the two others, formed a lattice with two molecules packed in order along the peptide backbone long axes, generating spacing that is longer than the length of a single peptide. Again, following a 5 h incubation of this film on $SBF_{1.5}$, the surface pressure increased by several millinewtons per meter (mN/m), a value significantly larger than that observed for the incubated PFD-5 and PFE-5 films (in accordance with the trend detected in isotherms measured after 18 h of incubation on $SBF_{1.5}$; see Figure 1). Interestingly, following this incubation and the concomitant increase in surface pressure, there was almost no change in the $d_{(0,1)}$ position measured by GIXD, providing additional evidence for the rigidity of the PPS monolayer being maintained during mineralization on $SBF_{1.5}$ solution (Table 1).

ATR-FTIR. Calcium phosphate adsorption to the peptide monolayers was monitored by ATR-FTIR spectroscopy. Peptide films were incubated for 12 days in a humidified incubator at 37 °C and then transferred horizontally to the ATR prism (see Experimental Section). On the basis of our previous experience with similar type of measurement,[20] this long period of time was considered necessary to detect ATR-FTIR signal of the phosphate groups adsorbed to the mineralizing peptide monolayers. Accordingly, all three peptide films transferred to the ATR prism after the 12 days incubation exhibited enhanced bands in the ∼900−1230 cm^{-1} (Figure 4),

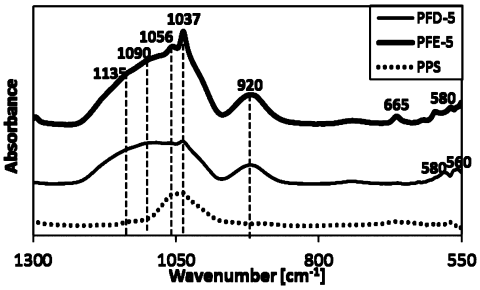

Figure 4. FTIR spectra of PFD-5, PFE-5 and PPS films transferred to ATR prizms at $\pi \sim 5$ mN/m from a $SBF_{1.5}$ interface after 12 days of incubation.

the υ_3 region, attributed to absorption of the P−O bond.[26] PFD-5 displayed a broad band at >1090 cm^{-1}, which may be attributed to PO_4^{3-} groups in amorphous calcium phosphate.[27,28] The 1037 cm^{-1} band, which appears distinct in the spectra, represents the strongest peak of octacalcium phosphate (OCP), carbonated apatite, and stoichiometric apatite.[29] The absorption peak at 920 cm^{-1} may be assigned to the υ_1 P−O symmetric stretches.[26,28] Additionally, absorption peaks observed in the 560−600 cm^{-1} region may be assigned to υ_4 P−O asymmetric bending mode.[30,31] The spectrum of PFE-5 shows similar features to that of PFD-5, with slightly enhanced intensity. The PPS spectrum appears weaker in general, as compared to the spectra of the other two peptides, and shows a main absorption band at ∼1037−1056 cm^{-1} and with almost no signal in the >1090 cm^{-1} region, which is characteristic of nonapatitic and amorphous calcium phosphate forms.[32]

DISCUSSION

Mineralization on monolayers incubated over SBF solution starts with the generation of calcium-phosphate nanometer-size clusters, namely, Posner particles,[33] that accumulate along with other ions at the templating surface and transform over time into the thermodynamically stable crystalline apatite form. These clusters are considered prenucleating forms that constitute the amorphous calcium phosphate phase. It has been proposed by the group of Sommerdijk[8] that a nucleating surface, in the form of a monolayer over SBF solution, induces structural and compositional changes that enable the denser packing of the clusters and their subsequent fusion to form amorphous calcium-phosphate. In the present study we focused on comparing the effect that different anionic groups, decorated on a β-sheet template, may have on early stages of calcium-phosphate mineralization.

The BAM images suggest that the PFD-5 peptide with the Asp side chains interacts immediately with the ions in the mineralizing solution, as compared to the two other peptides, PFE-5 and PPS, which appear to react more slowly. The images of PFD-5 on $SBF_{1.5}$-NI showed more pronounced film thickening, suggestive of both the immediate and excessive mineralization of the film, as compared to the other two peptides. BAM images of PFE-5 and PPS on $SBF_{1.5}$-NI also showed domains that appear to have different texture and overall gray levels that are slightly brighter than those obtained for the same films that formed on the water subphase. The mineralized PFD-5 film that formed over 18 h showed excessive and bright regions that appeared nonuniform, possibly also as a result of film folding. The mineralized films of PFE-5 and PPS incubated over $SBF_{1.5}$ showed fairly uniform textures that were brighter overall than the films imaged with no incubation.

The $\pi-A$ isotherms indicated that the $SBF_{1.5}$ had an immediate effect on all three peptides. PFD-5 showed a significant decrease in the collapse pressure on $SBF_{1.5}$-NI, and further changes in the isotherm shape were also observed after the time of incubation. The solution had a smaller effect on the two other peptides in terms of the limiting area per molecule; however, differences were clearly noted in the collapse state. Following incubation, both PFE-5 and PPS showed more significant changes in isotherm shape, with pronounced increase in the surface pressure in the most expanded state where films were left for incubation. The isotherms, therefore, provide the proof for immediate interactions with the ionic substances in the SBF solution that progressively build up on the peptide templates along the adsorption. BAM images of peptides PFE-5 and PPS incubated for 18 h on $SBF_{1.5}$ showed domains that are laterally larger (as compared to the domains detected on water), yet not as thick as those formed with PFD-5. The increase in surface pressure also suggests that the mineralized peptide domains grew in lateral dimensions due to mineral adsorption to the domains periphery (see Scheme3). Interestingly, there was a difference in the behavior of the PFE-5 and PPS incubated films evident in isotherms. The mineralized PFE-5 maintained the higher effective area along the compressed state, implying strong interactions between the adsorbed mineral and the peptide domains, which acted together in resisting the compression. By contrast, the PPS

Scheme 3. Schematic Representation of the Principal Differences in Mineralized PPS (left) and PFD-5 (right) Peptide Monolayers on $SBF_{1.5}$ Solution, Showing a More Uniform and Thinner Mineralized Layer on PPS, As Compared to an Apparently Thicker Mineral Layer on PFD-5[a]

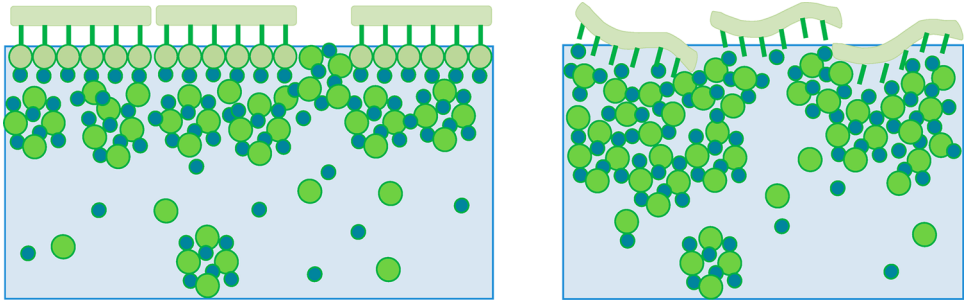

[a]Phosphate and calcium ions are represented by green and blue circles, respectively. Clusters of phosphate-calcium ions, known as Posner particles, that exist in the solution and participate in the buildup of the mineralized adsorbed layer, are represented by the grouped circles. The rigidity of the PPS template is designated by uniformly ordered peptide backbones at the interface that are maintained during the adsorption process. In addition, the scheme highlights that each divalent phosphate ion (light green circle) in the phosphoserine side chain may be neutralized by one calcium ion. The pronounced increase in surface pressure during PPS mineralization could be the result of film rigidity, along with adsorption of calcium-phosphate ions at the rim of peptide domains, in a manner that influences the apparent limiting area per molecule of the peptide. The PFD-5 monolayer is represented by distorted backbones, demonstrating the loss of order resulting from interactions with the adsorbed ions.

film appeared to show no resistance of the mineralized film to compression along the expanded state, which was followed by a compressed state at area per molecule similar to that of the peptide on water. This behavior suggests that the mineral adsorbed to the periphery of the PPS domains may have been easily desorbed in reaction to the condensation imposed along the compression in the expanded state in a manner that essentially left the peptide domains only to resist the compression along the compressed state.

GIXD provides further insight into the effect of $SBF_{1.5}$ on the peptides at the nanometer scale level as reflected in the repeat distance generated by the long axis of the peptides' lattice. The fact that the molecular order of the PFD-5 film, as indicated by the $d_{(0,1)}$ Bragg peak, could not be detected after incubation over $SBF_{1.5}$ suggests that the assemblies of this peptide are held by weaker intermolecular forces, such that the adsorbed ions led to their disruption. PFE-5, which on water shows crystalline compressibility similar to that of PFD-5, turned out to exhibit higher crystalline stability along the mineralization. PPS ordered domains were found to be highly resistant to compression on water, and these also maintained their rigidity after the adsorption of ions, as demonstrated by the diffraction pattern obtained following the incubation. The high resistance to compression of the PPS peptide monolayer could be the result of the steric differences between carboxyl and phosphate side chains. The larger PO_4^{2-} groups decorating PPS definitely contribute to the increased resistivity of these assemblies to compression, as compared to the COO^- groups that decorate PFE-5 and PFD-5. Attenuated total reflectance infrared (ATR-IR) measurements of mineralized film pulled out of the interface and undergoing dehydration, appear to be consistent with the in situ BAM, suggesting that the PPS peptide induced a thinner mineralized layer indicative by the rather weak absorption signals compared to the stronger spectrum of PFD-5 and PFE-5. The added value in these ATR-IR spectra is the information on the calcium-phosphate phases induced by the peptide templates. As the peak of the main absorption signal on PPS appears at ~1035 cm^{-1}, it suggests that the calcium-phosphate ions adsorbed by PPS formed the hydroxyapatite phase. Hence, although the thickness of the mineralized film on PPS appears to be smaller compared to the two other peptides, it induced the mineralization of the calcium-phosphate in a more unique manner, in the hydroxyapatite phase. The two other peptides induced thicker mineralized films that constitute amorphous calcium-phosphate and possibly other transient phases in addition to the hydroxyapatite phase.

The rather small thickness of the mineralized layer on PPS could also be the result of differences in the ionic charges of the hydrophilic amino acid side chains, with PPS being decorated by dianionic phosphate groups, as opposed to the monovalent acidic carboxyls decorating the other two peptides. It is possible that the phosphate groups in $SBF_{1.5}$ first become neutralized by the divalent calcium cations (see Scheme 3), turning essentially neutral in charge and then leading to smaller extent in adsorption of additional ions. By contrast, in PFD-5 and PFE-5 films, a calcium ion adsorbed to a carboxyl group needs an additional negative charge to stabilize, and that could result in various electrostatic interactions with Posner-like ionic aggregates from the SBF solution that lead to thicker ionic layers on PDF-5 and PFE-5.

CONCLUSIONS

Peptide PFD-5 template, which shows the highest compressibility value on SBF-NI and lost molecular order during mineralization according to GIXD, appears to interact faster and to a larger extent compared to the two other peptides with the mineralizing solution. The more rigid PFE-5 and PPS peptide films at the interface of the $SBF_{1.5}$ solution are capable of sustaining their structure along the ionic adsorption (Scheme 3). These more rigid films appear to form thinner mineralized layers, which in the case of PFE-5, constitute amorphous calcium phosphate together with apatite phase, and in PPS, according to IR spectra, the apatite phase only.

These results demonstrate differences in mineralized film morphology and peptide lattice behavior of β-sheet templates decorated by phosphate group side-chains, as compared to peptides decorated by carboxyl groups. Template rigidity, along with side chain type, were found to significantly alter the kinetics and extent of mineralization. In addition, the templates affected the morphology of the mineral-peptide system and the calcium-phosphate phase.

dx.doi.org/10.1021/jp305386e | J. Phys. Chem. B 2012, 116, 11197−11204

AUTHOR INFORMATION

Corresponding Author

*Phone: +972-8-6479043, Fax: +972-8-6477188. E-mail: hannarap@bgu.ac.il.

Notes

The authors declare no competing financial interest.

ACKNOWLEDGMENTS

This study was supported by the BIO−DISC cooperation in biotechnology between Germany (BMBF) and Israel (the Ministry of Industry, Trade& Labor and the Ministry of Science and Technology). We thank Hasylab, DESY for beam-time at beamline BW1, and funding from the European Community's Seventh Framework Programme (FP7/2007-2013) under grant agreement no. 226716.

REFERENCES

(1) Hunter, G. K.; Hauschka, P. V.; Poole, A. R.; Rosenberg, L. C.; Goldberg, H. A. *Biochem. J.* **1996**, *317*, 59−64.
(2) Young, M. F.; Kerr, J. M.; Ibaraki, K.; Heegaard, A. M.; Robey, P. G. *Clin. Orthop. Relat. Res.* **1992**, *281*, 275−294.
(3) Duffy, D. M.; Travaille, A. M.; Kempen, H. van; Harding, J. H. *J. Phys.Chem. B* **2005**, *109*, 5713−5718.
(4) Volkmer, D.; Fricke, M.; Agena, C.; Mattay, J. *J. Mater. Chem.* **2004**, *14*, 2249−2259.
(5) Colfen, H.; Mann, S. *Angew. Chem., Int. Ed.* **2003**, *42*, 2350−2365.
(6) Addadi, L.; Raz, S.; Weiner, S. *Adv. Mater.* **2003**, *15*, 959−970.
(7) Beniash, E.; Metzler, R. A.; Lam, R. S. K.; Gilbert, P. *J. Struct. Biol.* **2009**, *166*, 133−143.
(8) Dey, A.; Bomans, P. H. H.; Müller, F. A.; Will, J.; Frederik, P. M.; De With, G.; Sommerdijk, N. A. J. M. *Nat. Mater.* **2010**, *9*, 1010−1014.
(9) Beniash, E.; Aizenberg, J.; Addadi, L.; Weiner, S. *Proc. R. Soc. B.* **1997**, *264*, 461−465.
(10) Politi, Y.; Arad, T.; Klein, E.; Weiner, S.; Addadi, L. *Science* **2004**, *306*, 1161−1164.
(11) Crane, N. J.; Popescu, V.; Morris, M. D.; Steenhuis, P.; Ignelzi, M. A., Jr. *Bone* **2006**, *39*, 434−442.
(12) Xu, G. F.; Aksay, I. A.; Groves, J. T. *J. Am. Chem. Soc.* **2001**, *123*, 2196−2203.
(13) Volkmer, D.; Fricke, M.; Huber, T.; Sewald, N. *Chem. Commun.* **2004**, *16*, 1872−1873.
(14) Bekele, H.; Fendler, J. H.; Kelly, J. W. *J. Am. Chem. Soc.* **1999**, *121*, 7266−7267.
(15) DeOliveira, D. B.; Laursen, R. A. *J. Am. Chem. Soc.* **1997**, *119*, 10627−10631.
(16) Meegan, J. E.; Aggeli, A.; Boden, N.; Brydson, R.; Brown, A. P.; Carrick, L.; Brough, A. R.; Hussain, A.; Ansell, R. J. *Adv. Funct. Mater.* **2004**, *14*, 31−37.
(17) Bertrand, M.; Brack, A. *Chem.—Eur. J.* **2000**, *6*, 3452−3455.
(18) Chevalier, N. R.; Chevallard, C.; Goldmann, M.; Brezesinski, G.; Guenoun, P. *Cryst. Growth. Des.* **2012**, *12*, 2299−2305.
(19) Cavalli, S.; Popescu, D. C.; Tellers, E. E.; Vos, M. R. J.; Pichon, B. P.; Overhand, M.; Rapaport, H.; Sommerdijk, N. A. J. M.; Kros, A. *Angew. Chem., Int. Ed.* **2006**, *45*, 739−744.
(20) Segman-Magidovich, S.; Grisaru, H.; Gitli, T.; Levi-Kalisman, Y.; Rapaport, H. *Adv. Mater.* **2008**, *20*, 2156−2161.
(21) Rapaport, H.; Kuzmenko, I.; Berfeld, M.; Kjaer, K.; Als-Nielsen, J.; Popovitz-Biro, R.; Weissbuch, I.; Lahav, M.; Leiserowitz, L. *J. Phys. Chem. B* **2000**, *104*, 1399−1428.
(22) Rapaport, H.; Kjaer, K.; Jensen, T. R.; Leiserowitz, L.; Tirrell, D. A. *J. Am. Chem. Soc.* **2000**, *122*, 12523−12529.
(23) Isenberg, H.; Kjaer, K.; Rapaport, H. *J. Am. Chem. Soc.* **2006**, *128*, 12468−12472.
(24) Vaiser, V.; Rapaport, H. *J. Phys. Chem. B* **2010**, *115*, 50−56.
(25) Kokubo, T.; Ito, S.; Huang, Z. T.; Hayashi, T.; Sakka, S.; Kitsugi, T.; Yamamuro, T. *J. Biomed. Mater. Res.* **1990**, *24*, 331−343.
(26) Trommer, R. M.; Santos, L. A.; Bergmann, C. P. *Surf. Coat. Technol.* **2007**, *201*, 9587−9593.
(27) Rehman, I.; Bonfield, W. *J. Mater. Sci.: Mater. Med.* **1997**, *8*, 1−4.
(28) Fowler, B. O. *Inorg. Chem.* **1974**, *13*, 194−207.
(29) Rey, C.; Shimizu, M.; Collins, B.; Glimcher, M. *Calcif. Tissue Int.* **1991**, *49*, 383−388.
(30) Liu, Y.; Hou, D.; Wang, G. *Mater. Chem. Phys.* **2004**, *86*, 69−73.
(31) Ou-Yang, H.; Paschalis, E. P.; Boskey, A. L.; Mendelsohn, R. *Biopolymers* **2000**, *57*, 129−139.
(32) Rau, J. V.; Fosca, M.; Komlev, V. S.; Fadeeva, I. V.; Albertini, V. R.; Barinov, S. M. *Cryst. Growth Des.* **2010**, *10*, 3824−3834.
(33) Posner, A. S.; Betts, F. *Acc. Chem. Res.* **1975**, *8*, 273−281.